Nadph oxidase regulates alveolar epithelial sodium channel activity and lung fluid balance in vivo via O_2^- signaling

Preston Goodson, Amrita Kumar, Lucky Jain, Kousik Kundu, Niren Murthy, Michael Koval and My N. Helms

Am J Physiol Lung Cell Mol Physiol 302:L410-L419, 2012. First published 9 December 2011; doi:10.1152/ajplung.00260.2011

Am J Physiol Lung Cell Mol Physiol 302: L410–L419, 2012.
First published December 9, 2011; doi:10.1152/ajplung.00260.2011.

Nadph oxidase regulates alveolar epithelial sodium channel activity and lung fluid balance in vivo via O_2^- signaling

Preston Goodson,[1] Amrita Kumar,[1] Lucky Jain,[1,2] Kousik Kundu,[4] Niren Murthy,[4] Michael Koval,[3] and My N. Helms[1,2]

[1]*Department of Physiology and* [2]*Department of Pediatrics Center for Developmental Lung Biology at Children's Healthcare of Atlanta,* [3]*Department of Medicine and Cell Biology, Emory University; and* [4]*Wallace H. Coulter Department of Biomedical Engineering, Georgia Institute of Technology, Atlanta, Georgia*

Submitted 5 August 2011; accepted in final form 3 December 2011

Goodson P, Kumar A, Jain L, Kundu K, Murthy N, Koval M, Helms MN. Nadph oxidase regulates alveolar epithelial sodium channel activity and lung fluid balance in vivo via O_2^- signaling. *Am J Physiol Lung Cell Mol Physiol* 302: L410–L419, 2012. First published December 9, 2011; doi:10.1152/ajplung.00260.2011.—To define roles for reactive oxygen species (ROS) and epithelial sodium channel (ENaC) in maintaining lung fluid balance in vivo, we used two novel whole animal imaging approaches. Live X-ray fluoroscopy enabled quantification of air space fluid content of C57BL/6J mouse lungs challenged by intratracheal (IT) instillation of saline; results were confirmed by using conventional lung wet-to-dry weight ratios and Evans blue as measures of pulmonary edema. Visualization and quantification of ROS produced in lungs was performed in mice that had been administered a redox-sensitive dye, hydro-Cy7, by IT instillation. We found that inhibition of NADPH oxidase with a Rac-1 inhibitor, NSC23766, resulted in alveolar flooding, which correlated with a decrease in lung ROS production in vivo. Consistent with a role for Nox2 in alveolar fluid balance, $Nox2^{-/-}$ mice showed increased retention of air space fluid compared with wild-type controls. Interestingly, fluoroscopic analysis of C57BL/6J lungs IT instilled with LPS showed an acute stimulation of lung fluid clearance and ROS production in vivo that was abrogated by the ROS scavenger tetramethylpiperidine-*N*-oxyl (TEMPO). Acute application of LPS increased the activity of 20 pS nonselective ENaC channels in rat type 1 cells; the average number of channel and single-channel open probability (*N*Po) increased from 0.14 ± 0.04 to 0.62 ± 0.23. Application of TEMPO to the same cell-attached recording caused an immediate significant decrease in ENaC *N*Po to 0.04 ± 0.03. These data demonstrate that, in vivo, ROS has the capacity to stimulate lung fluid clearance by increasing ENaC activity.

small G protein; Rac1; LPS; chest X-ray; intratracheal instillation; amiloride

ALVEOLAR TYPE 1 (AT1) and type 2 (AT2) cells comprise the alveolar epithelium, which together serve to separate the luminal air space from the vasculature. The role of AT1 and AT2 cells in gas exchange and surfactant production is well established (5, 54). We have recently shown that both cell types express functional epithelial sodium channels (ENaC) using single-channel patch-clamp analysis (15, 17). Sodium uptake from the luminal surface generates the electroosmotic flow that pulls water molecules across the alveolar epithelium and, hence, maintains an appropriately moist luminal space for effective gas exchange. As such, regulation of lung ENaC is of utmost importance for normal respiration. Transgenic mice that lack α-ENaC expression die within days of birth, because of an inability to clear lung fluid (22). Interestingly, this lethal phenotype can be rescued by epigenetically expressing ENaC (21). Conversely, hyperactive sodium channel activity aberrantly dries the airways and leads to the excessively thick mucus present in children with cystic fibrosis disease (33, 46, 58). Although ENaC plays an important role in health and disease, the signal transduction pathways that regulate this ion channel remain largely unknown in both AT1 and AT2 cells.

Fetal lungs transition from low to high oxygen tension at birth as they transition from a fluid-secreting organ to an organ that can actively reabsorb salt and water. Thus oxygen signaling has been implicated in regulating lung ENaC (3, 37, 38, 40–43, 50). Oxygen could serve as a signaling molecule following reduction to superoxide anion, O_2^-. Superoxide anions are usually dismutated to H_2O_2, or they react with nitric oxide to form peroxynitrite; all of these molecules have been shown to be important regulators of ENaC activity (14, 19, 29, 34, 52, 56). We have recently shown in vitro that sequestering O_2^- with 2,2,6,6-tetramethylpiperidine-*N*-oxyl (TEMPO) inhibits ENaC activity (56), and conversely that increasing amounts of O_2^- by using a mix of hypoxanthine and xanthine oxidase, or superoxide dismutase inhibitors, increases ENaC activity (15, 56). The focus of this study is to determine whether these pathways play an important role in regulating lung fluid in vivo.

One of the best characterized sources of cellular reactive oxygen species (ROS) is via NADPH oxidase production of O_2^- (reviewed in Ref. 28). In the present study, we test the hypothesis that the Nox family of NADPH oxidases plays an integral role in regulation of ENaC. NADPH oxidases are membrane-bound enzyme complexes, with seven major isoforms identified (Nox1–5 and Duox1–2). Each isoform is structurally related to the others, and all are capable of releasing ROS. The signaling pathways that govern NADPH oxidase significantly overlap with established ENaC regulatory pathways. For example, full assembly and activation of Nox2 requires protein kinase signaling, lipid metabolizing enzymes, and conversion of Rac1 from the GDP-bound to the activated GTP-bound form. Only after full stimulation of these signaling molecules can the cytosolic regulatory proteins of Nox1–3 isoforms (p40phox, p47phox, and p67phox) associate with and activate the catalytic domains of gp91phox, for ROS production. Interestingly, the kinases and signaling molecules needed for regulation of Nox isoforms, such as phosphatidylinositol 3-kinase, phosphatidylinositols, and Rac1, have also been shown to be important components of ENaC signaling (10, 16, 32). Despite the significant overlap in signal transduction

Address for reprint requests and other correspondence: M. N. Helms, Dept. of Physiology, Center for Cell and Molecular Signaling, 615 Michael St., Suite 646, Atlanta, GA 30322 (e-mail: mhelms@emory.edu).

between Nox2 and ENaC activation, the intimate relationship between NOX release of O_2^- and ENaC activity has not been fully investigated. In the present study, we utilized multimodal animal imaging and single-channel patch-clamp analysis to study the role of NADPH oxidase in lung fluid clearance.

MATERIAL AND METHODS

Animal care. Wild-type C57BL/6J mice (8 and 12 wk old) and 8-wk-old C57BL/6J mice with Nox2 gene expression disrupted (B6.129S-Cybb^{tm1Din}/J) were purchased from The Jackson Laboratory (Bar Harbor, ME) and housed with access to standard diet and water ad libitum. All animal protocols and handling conform to National Institutes of Health animal care and use guidelines, as approved by Emory University Institutional Animal Care and Use Committee.

IT instillations. Intratracheal (IT) instillation of solute into the alveolar air space has been described in Ref. 18. Mice were anesthetized with an intraperitoneal injection of 15 mg/kg xylazine (Anased 100 mg/ml, Lloyd Laboratories; Shenandoah, IA) and 125 mg/kg ketamine (ketamine hydrochloride injection USP 50 mg/ml, Bioniche Pharma USA; Lake Forest, IL) prepared in phosphate-buffered saline (PBS, pH 7.4; Invitrogen, Grand Island, NY) for a final intraperitoneal injection volume of 250 μl per 20-g mouse. The instillate vehicle for all experiments consisted of 140 mM NaCl, 5 mM KCl, 1 mM $CaCl_2$, and 10 mM HEPES with pH = 7.4; hereafter referred to as control saline. The osmolality of this saline solution is 319 mosmol/kgH_2O, which is near the reported plasma osmolality of mice (1, 12). Tracheal instillation volumes of 5 μl per gram of body weight (100 μl final volume in 20 g C57BL/6J mice) were delivered by use of a 26-gauge, 5/8-in. needle and a 1-ml syringe. Experimental groups included instillations of 100 μl saline, LPS (1 mg/ml), 1 mM amiloride, 250 μM 2,2,6,6-tetramethylpiperidine 1-oxyl (TEMPO), or 100 μM NSC23766. All compounds are available commercially. Following instillation, the incision site was closed and animals were immediately placed into the imaging station described below under *fluoroscopy*.

Fluoroscopy. Animals were X-rayed or imaged for fluorescence signal by using an In-Vivo MS FX Pro small animal imager (Carestream Health; Rochester, NY) with an E-Z Anesthesia unit (Palmer, PA) attached to deliver oxygen and 2% isoflurane. Ambient temperature in the imager was elevated ~4° above RT to keep the animals warm. Animals were X-ray imaged at 5-min intervals up to 240 min with an acquisition period of 120 s and kept on oxygen mixed with gas anesthesia for the duration of imaging. X-ray settings were 2×2

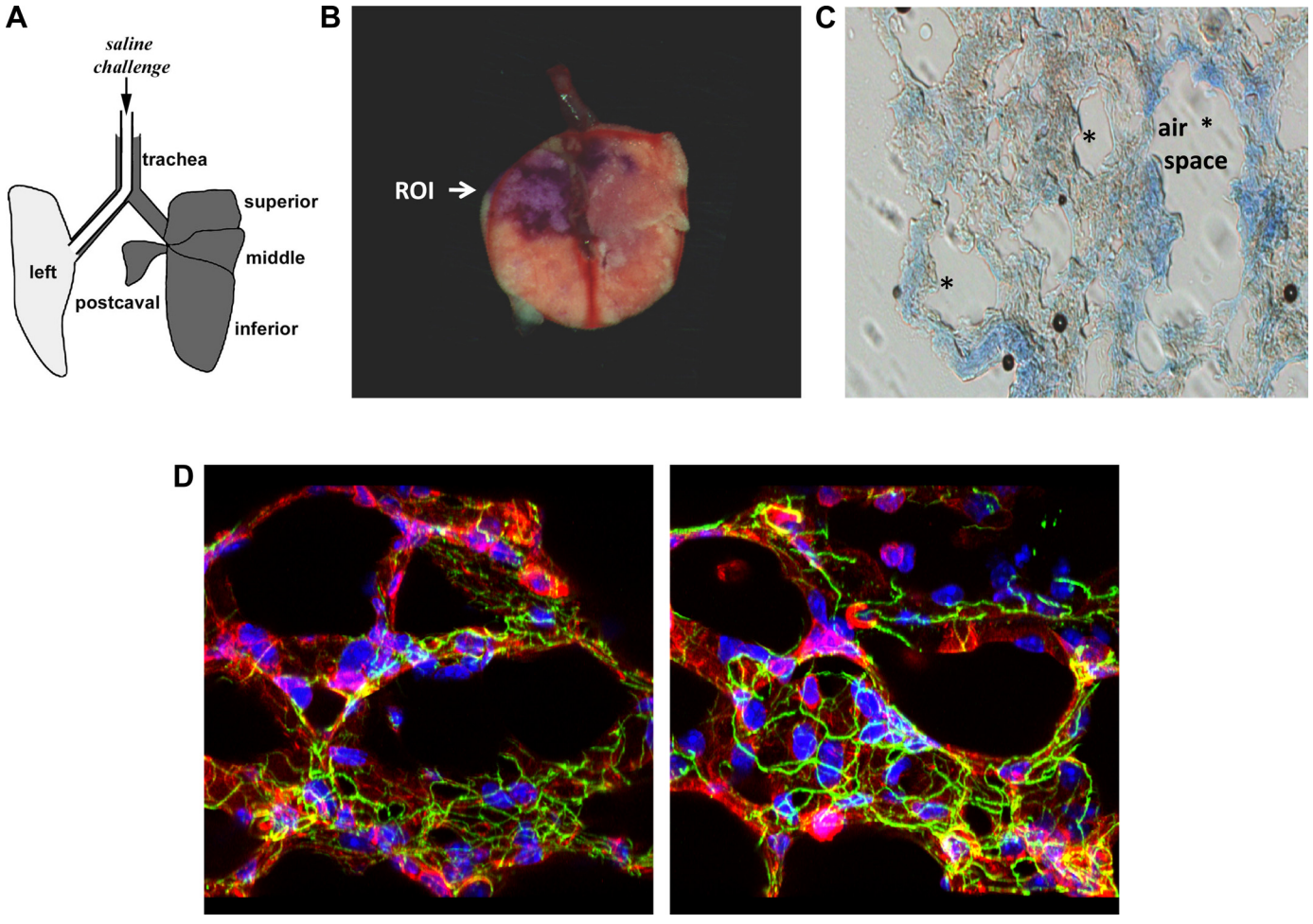

Fig. 1. Distribution and detection of intratracheally (IT) instilled saline in C57BL/6J mouse lung. *A*: schematic of mouse lung, indicating IT administration of a saline challenge specifically into the left lobe. *B*: mouse lung instilled IT with 25 μl bromophenol blue dye, excised, and photographed to show region of dye accumulation in the upper left lung lobe, indicated here as region of interest (ROI). *C*: 10-μm tissue section prepared from the lung shown in *B*, demonstrating that bromophenol blue dye-labeled instillate reached the distal alveolar air space (*). *D*: confocal images of uninstilled (*left*) and 100 μl saline-instilled (*right*) left lung lobes fluorescently labeled with anti-zonula occludens-1 antibody to label tight junctions [488 nm (green) excitation], rhodamine phalloidin to label actin [538 nm (red) excitation]; and 4,6-diaminido-2-phenylindole (DAPI) to label nuclei [360 nm (blue) excitation]. IT saline administration did not induce gross lung damage.

binning, 180-mm field of view (FOV), 149 μA X-ray current, 35 kVp, and 0.4-mm aluminum filter.

X-ray density was quantified by using Carestream Health MI software with a 5-mm^2 region of interest (ROI). In all whole animal studies, the ROI was the upper left lobe of the lung (see Fig. 1). In fluoroscopic studies, all 5-mm^2 ROI placements were caudal to the third rib on the left side of the chest X-ray. All fluoroscopic ROIs were background corrected and normalized to the initial X-ray intensity (I_o) to make comparisons between time points and experimental groups. Specifically, changes in lung fluid volume are expressed as $I-I_o$, where I is the X-ray density at a respective time point and I_o is the initial X-ray density following saline challenge.

Fluorescent imaging. Thoracic fur was removed prior to imaging. The redox-sensitive dye hydrocyanine (Cy 7; 2 mM) was reconstituted in saline solution and IT instilled into C57BL/6J lung after 4 h following LPS, LPS+ NSC23766, NSC23766, or saline instillation. Animals were placed into the small rodent imager configured for epi-illumination and fluorescence detection. Specifically, imager settings were 140-mm FOV, 4×4 binning, 700 nm excitation, and 830 nm emission. Data were collected by a charge-coupled device camera during a 5-min acquisition period and ROI was analyzed by use of Carestream Health Multispectral (MI) Software.

The fluorescence intensity of ROS-activated (Cy7) was also quantified from the upper left lobe of the lung by use of Carestream Health MI software and expressed as photons per second per square centimeter.

Statistical analysis. All data are summarized as means ± SE. Single comparisons were performed by Student's *t*-test. Multiple comparisons were performed by one-way ANOVA followed by the Holms test for pairwise comparisons. *P* values of <0.05 were regarded as statistically significant.

Detection of 0.5% bromophenol dye in the alveoli. After IT instillation of bromophenol blue dye under anesthesia, mice were exsanguinated by cutting the renal artery, and lungs were perfused via the right ventricle with PBS. Subsequently, lungs were excised from the thoracic cavity and covered with a thin layer of optimal cutting temperature (OCT) compound. Lung tissue embedded in OCT was snap frozen in liquid N_2-cooled isopentane and sectioned in a cryostat. Bromophenol blue was detected in the alveoli by use of an inverted IX-70 Olympus microscope.

Confocal microscopy. Lung tissue slices were prepared as described in Ref. 15. Cells were fixed in 2% paraformaldehyde before immunolabeling with anti-zona occludin antibody used at a 1:1,000-fold dilution. Anti-rabbit secondary antibodies conjugated to Alexa 488 (Molecular Probes) were used at a 1:20,000-fold dilution. Lung tissues were also counterstained with 1:1,000 phalloidin (Upstate) prior to being mounted on glass coverslips with 4,6-diaminido-2-phenylindole Vectashield (Vector Laboratories). Labeled cells were imaged by use of an Olympus BX61WI confocal microscope and Fluoview FV10-ASW 1.7 software.

Electrophysiology. AT1 cells were accessed from a live lung tissue preparation and patch clamped as described in Ref. 17. Briefly, 250-μm lung slices were prepared from agarose-instilled rat lungs by use of a vibrating microtome and transferred to 50:50 ice-cold DMEM/F-12 media containing FBS (10%), L-glutamine (2 mM), dexamethasone (1 μM), gentamicin (84 μM), and penicillin-streptomycin (20 U/ml) prior to patch-clamp analysis. Following GΩ seal formation between the apical membrane and patch-clamp electrode, a control recording period (5 min) was obtained prior to adding LPS (1 μg/ml) and then TEMPO (250 μM) to the same cell-attached patch-clamp recording to determine the role of ROS signaling on lung ENaC activity. The product of the number of channels (*N*) and the single-channel open probability (P_o) was calculated by use of Clampfit 10.1 software (Molecular Devices).

Wet-to-dry lung weight ratios. Under ketamine and xylazine anesthesia (described above) C57BL/6J lungs were IT instilled with 100 μl saline. The lungs were excised and weighed 30 min following instillation. Lungs were dried at 60°C for 48 h, then weighed again to obtain the wet-to-dry weight ratios.

Evans blue-labeled albumin measurements. Twelve-week-old mice were tracheally instilled (as described above) with solution containing 5% bovine serum albumin (BSA) and Evans blue dye (0.1 mg/ml). Alveolar fluid clearance (AFC) was assessed 60 min after instillation by measuring the change in concentrations of alveolar Evans blue-labeled albumin. As described in Refs. 44, 53, AFC was calculated as follows:

$$AFC = [(Vi - Vf)/Vi] \times 100,$$

where Vi is the volume of instilled Evans blue-labeled albumin and Vf is the final alveolar fluid calculated as follows:

$$Vf = (Vi \times EBi)/EBf,$$

where EB is the concentration of Evans blue-labeled albumin in the instilled solution (i) and the final alveolar fluid (f). Protein concentration was determined with the use of spectrophotometry.

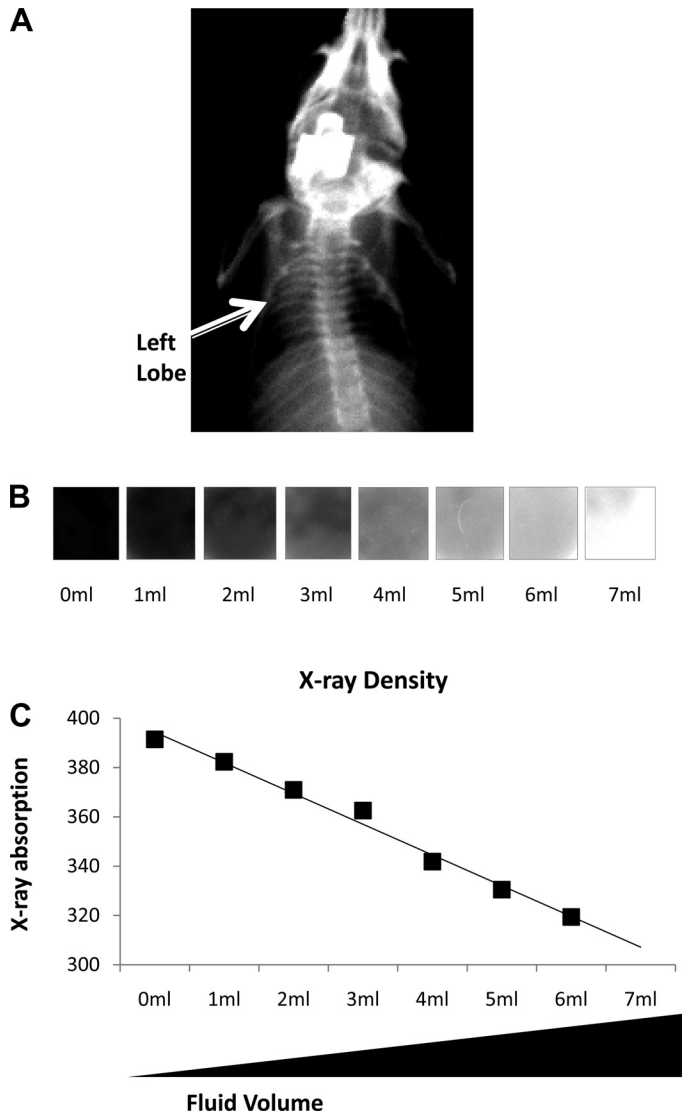

Fig. 2. Air space fluid is opaque in X-ray imaging. *A*: high-resolution X-ray imaging of C57BL/6J mice IT instilled. Arrow points to a fluid-filled ROI in the upper left lung lobe, which produces a cloudy white image due to X-ray attenuation. By contrast, air-filled lobes appear darker and are penetrated by X-rays. *B* and *C*: X-ray imaging of 0–7 ml saline in a 35-mm plastic petri dish demonstrated a linear increase in X-ray opacity with increasing fluid volume.

RESULTS

Distribution and detection of intratracheally instilled saline in C57BL/6J mouse lung. We and others have shown that IT instillation of solutes serves as an effective and minimally invasive technique for targeted delivery of compounds into lungs (9, 18, 31, 48, 55). In Fig. 1*A*, we show a schematic of the five lobes of mouse lung and the site of IT instillation used to localize the site of fluid accumulation. Accordingly, 25 μl tracheally instilled bromophenol blue dye accumulates in the upper left lobe of the excised lung (Fig. 1*B*). From the same lung shown in 1*B*, 10-μm cryoslices were prepared to verify that the small volume of instilled dye uniformly extends into the distal regions (alveoli) of the left lobe (Fig. 1*C*). This treatment did not have a significant effect on lung morphology, since the localization of a tight junction protein, zonula occludens-1 (ZO-1), and F-actin did not differ significantly between uninstilled (*left*) and 100 μl saline-instilled portions of the lung (Fig. 1*D*). That ZO-1 and actin labeling remained largely unchanged indicates that the barrier property of the alveolar epithelium remained intact and that a single saline challenge does not cause gross lung damage. The upper left lobe of the lung is the consistent site of fluid accumulation following IT instillation (35, 48). As such, we designate this area of the lung as the ROI in all subsequent studies.

Air space fluid is opaque in X-ray imaging. Fluid attenuates X-ray photons. As such, soft tissue and fluid filled compartments appear more opaque (white) than air-filled compartments, which, in contrast, appear black. This is demonstrated in Fig. 2*A*, which shows an X-ray image taken from a live C57BL/6J mouse following IT saline instillation into the upper left lobe of the lung (ROI). Between the ribs, the ROI has a cloudy, white appearance compared with the uninstilled right lobes of the lung. To confirm that this method gives us a quantitative method to measure fluid volume, we X-ray imaged

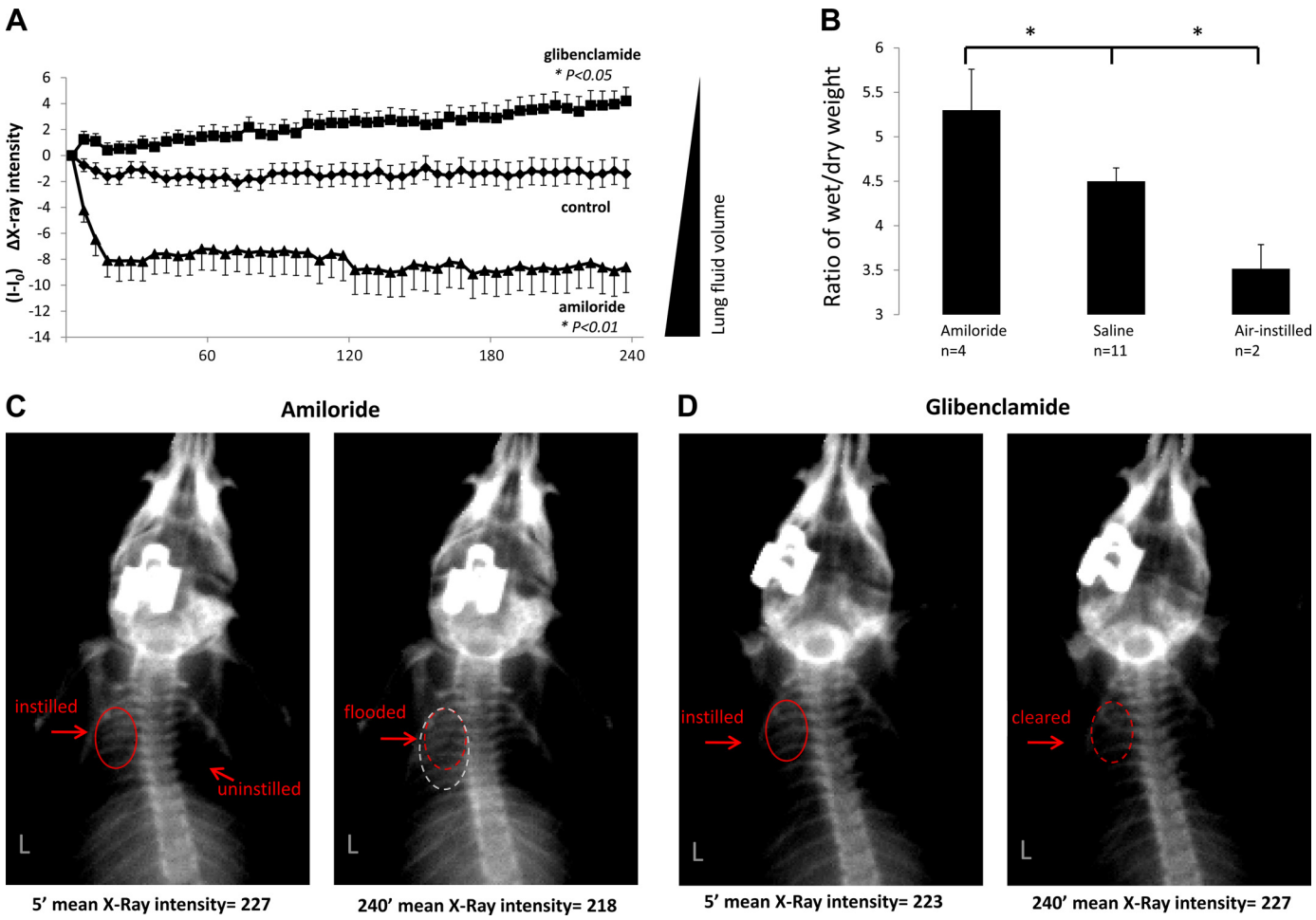

Fig. 3. X-ray fluoroscopy enabled in vivo imaging of lung fluid. *A*: 3-mo-old C57BL/6J mice were challenged by IT instillation with 100 μl of either control saline ($n = 10$), 1 mM glibenclamide ($n = 10$), or 1 mM amiloride ($n = 10$). The mice were imaged by X-ray fluoroscopy and quantified by $I-I_o$, where I_o is the X-ray intensity at an ROI immediately after instillation and I is the intensity at a given time following instillation. Each point represents a 2-min rolling average of X-ray intensity measurements corresponding to lung air space fluid volume. Amiloride instilled into C57BL mice significantly impaired the clearance of IT saline challenge compared with control animals instilled with an equal volume of control saline solution at all time points following I_o; $^*P < 0.01$. By contrast, glibenclamide inhibition of chloride channels effectively blocked secretion and enhanced fluid clearance at all time points following I_o. ($^*P < 0.05$) *B*: conventional wet-to-dry lung weight ratio measurements confirmed that amiloride inhibited lung fluid clearance 30 min postinstillation and correlate with in vivo X-ray fluoroscopic measurements ($^*P < 0.05$). *C* and *D*: representative X-ray images of amiloride and glibenclamide instilled lung 5 and 240 min postinstillation. ROI is circled in the left lobe of the lung. X-ray opacity and area of alveolar flooding (indicated by gray circle) increases 240 min following amiloride instillation. The ROI is more X-ray dense 240 min following glibenclamide instillation. Mean X-ray intensities of ROI reported under each figure.

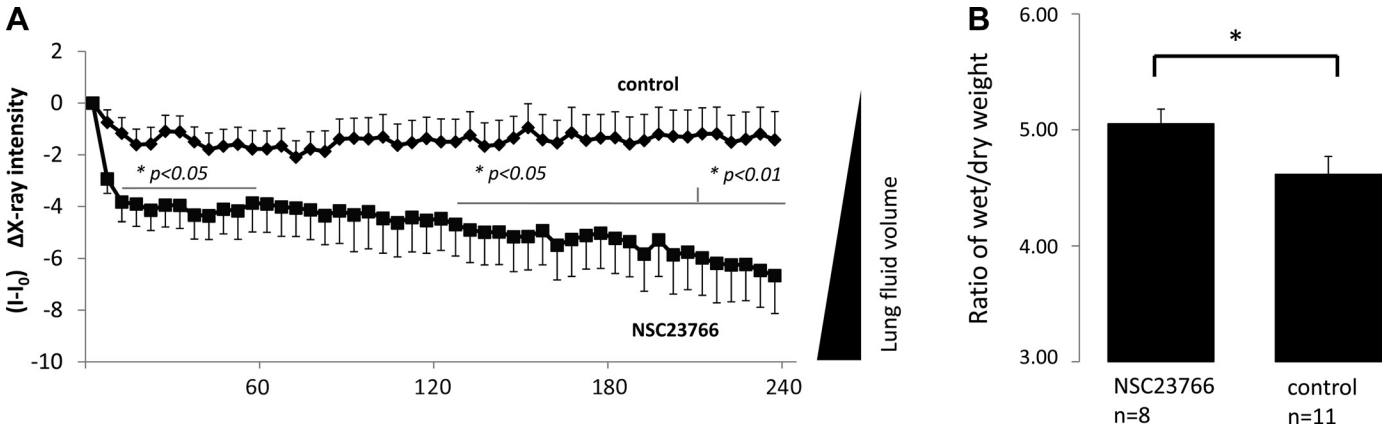

Fig. 4. Rac1 inhibition attenuated lung fluid clearance in vivo. *A*: C57BL/6J mice were challenged by IT instillation with 100 μl of either control saline (n = 10) or a Rac inhibitor compound 100 μM NSC23766 (n = 10). Mice treated with NSC23766 had significantly increased lung fluid volume, compared with control animals. *$P < 0.05$. *B*: wet-to-dry lung weight ratio measurements confirm that NSC23766 inhibited fluid clearance 30 min following instillation. *$P < 0.05$.

plastic 35-mm culture dishes containing fluid volumes ranging from 0 to 7 ml (Fig. 2, *B* and *C*), which showed a linear increase in X-ray opacity (lower density of X-ray transmission) with increasing fluid volume. On the basis of this relationship between fluid volume and X-ray absorption, we are able to track changes in lung fluid volume.

Air space fluid volumes correspond to altered lung ion transport properties. Activation of amiloride-sensitive sodium channels serves as the major pathway for salt and water reabsorption across the alveolar epithelium and out of the airways (4, 11, 12, 57). Conversely, outward flow of anions via CFTR influences the rate of pulmonary secretion driving in a net increase in lung airway fluid (7). To assess the utility of X-ray fluoroscopic imaging to assess lung liquid volume, we examined 12-wk-old C57BL6 mice that were IT instilled with either 140 mM saline alone, saline containing 1 mM amiloride (to inhibit ENaC), or saline containing 1 mM glibencamide (to block CFTR). The mice were challenged with 5 μl per gram body weight (~100 μl total). Immediately following IT instillation, animals were imaged by using a 2-min exposure every 5 min for a total of up to 240 min. X-ray intensities were quantified by $I-I_o$, where I_o is the X-ray intensity at an ROI immediately after instillation and I is the intensity at a given time following instillation. Thus $I-I_o$ decreases with increasing air space fluid volume (Fig. 3).

Consistent with previously published reports, real-time X-ray imaging of the lungs showed that blocking ENaC activity with amiloride (n = 10) significantly slowed the rate of fluid reabsorption compared with control animals instilled with equal volume saline (n = 10) (Fig. 3*A*). In Fig. 3, *C* and *D*, we show representative chest X-rays obtained 5 and 240 min after instillation of amiloride and glibenclamide. We also validated our X-ray fluoroscopic approach by measuring lung wet-to-dry weight ratios following IT instillation of saline and amiloride by comparison with mock-instilled lungs. As shown in Fig. 3*B*, mice with IT instilled amiloride had the highest levels of edema, consistent with our findings by live X-ray fluoroscopy.

We also examined the acute effect of glibenclamide, a blocker of CFTR transport (45), on lung fluid content. Blocking chloride channel activity significantly increased air space X-ray density (n = 10, $P < 0.05$), consistent with a decrease in lung fluid accumulation due to continued absorption combined with inhibited fluid secretion. Thus the nearly consistent $I-I_o$ values measured for saline-instilled animals are likely to reflect a steady-state equilibration between rates of fluid absorption and secretion.

Rac1 inhibition attenuated lung fluid clearance in vivo. Using single-channel patch-clamp analysis and dihydroethidium labeling, we have recently shown that the specific Rac1 inhibitor NSC23766 significantly decreases ENaC activity in both AT1 and AT2 cells and reduces cellular production of O_2^- (49). To determine whether these measurements at the individual cell level translate into net changes in lung fluid balance, we assessed the clearance of 100 μl 1 μM NSC23766 IT instilled into C57BL/6J mice (n = 10). As shown in Fig. 4*A*, mice IT instilled with NSC23766 failed to clear the saline challenge compared with control-instilled animals at several time points between I_o and 240 min. We verified the X-ray

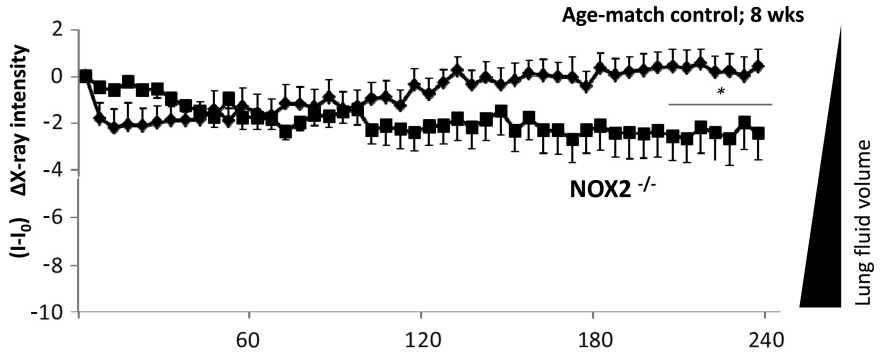

Fig. 5. NADPH oxidase 2-deficient mice have impaired lung fluid clearance. Eight-week-old $Nox2^{-/-}$ mice (n = 7) showed diminished clearance of a 100-μl saline IT challenge compared with age-matched control mice (n = 10), over a 4-h period. *$P < 0.05$.

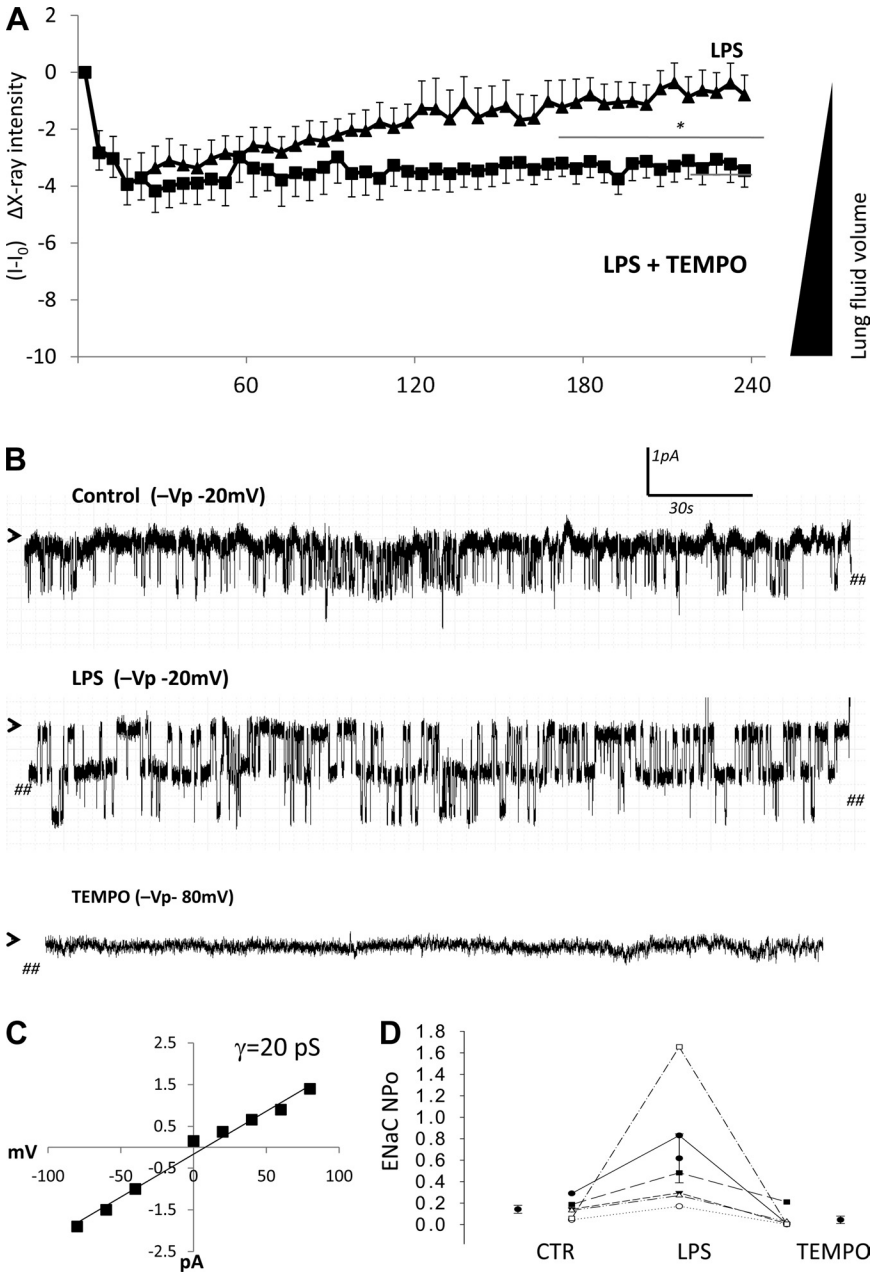

Fig. 6. Lipopolysaccharide (LPS)-stimulated O_2^- production promotes epithelial sodium channel (ENaC) activity and regulates lung fluid volume in vivo. *A*: C57BL/6J mice were challenged by IT instillation with 100 μl 1 mg/ml LPS ($n = 10$) or LPS + 250 μM 2,2,6,6-tetramethylpiperidine 1-oxyl (TEMPO; $n = 10$). In both cases, there was an initial increase in air space fluid volume; however, fluid clearance by LPS instilled animals was abrogated by TEMPO treatment ($^*P < 0.05$). *B*: representative cell-attached patch-clamp recording of an alveolar type 1 cell at −Vp (−20 mV) holding potential before LPS treatment (*top trace*) and acutely following 1 mg/ml LPS treatment (*middle trace*). In the same cell-attached patch-clamp recording, TEMPO was added, which sequestered O_2^- and significantly decreased Na current (*bottom trace*). Downward deflections from arrows (indicating closed state) are representative of inward current. Breaks in continuous cell recording are denoted by ##. *C*: slope conductance of a representative nonselective cation channel shown (*C*) is 20 pS. *D*: single-channel data analysis of ENaC activity in continuous patch-clamp recording demonstrates a significant increase in the number of open ENaC (*N*Po) abrogated by TEMPO. At baseline, ENaC had *N*Po = 0.14 ± 0.04, which significantly increased to 0.62 ± 0.22 following LPS treatment with LPS ($P < 0.05$). TEMPO immediately decreased ENaC *N*Po to 0.04 ± 0.03, which statistically differs from control (CTR) and LPS average values, $n = 6$; $P < 0.05$; Vp, pipette potential.

fluoroscopic measurements of fluid clearance using wet-to-dry weight ratios, which gave comparable results (Fig. 4*B*).

NADPH oxidase 2-deficient mice have impaired lung fluid clearance. Although Rac1 is implicated in several physiological responses, we hypothesized that Rac1 stimulates production of ROS derived from NADPH oxidase to stimulate lung ion transport. We tested this hypothesis by assessing the ability of Nox2-deficient mice ($Nox2^{-/-}$) to clear a saline challenge. As shown in Fig. 5, 8-wk-old $Nox2^{-/-}$ mice challenged with 5 μl saline per gram showed an impaired ability to clear IT instilled saline ($n = 8$) compared with 8-wk-old wild-type mice ($n = 10$).

LPS-stimulated O_2^- production promotes ENaC activity and regulates lung fluid volume in vivo. LPS is a known activator of NADPH oxidase activity that works through activation of Rac1 (23, 25). Thus we examined the ability of 12-wk-old C57BL/6J mice to clear IT instilled 100 μl of LPS (1 μg/μl). In a separate group of animals, we coinstilled TEMPO to sequester any ROS generated by instilled LPS. As shown in Fig. 6*A*, LPS immediately increased alveolar flooding. However, roughly 30 min after challenge, the LPS-instilled animals showed increased fluid clearance ($n = 10$). By contrast, mice cotreated with TEMPO did not ($n = 10$). Thus, by scavenging ROS, we abolished the ability of IT instilled LPS to acutely stimulate lung fluid clearance.

For the clearance measurements in Fig. 6*A*, we found that X-ray fluoroscopy was significantly more sensitive than wet-to-dry weight measurements, which were unable to detect a significant inhibition of LPS-induced fluid clearance by TEMPO (P. Goodson and M. N. Helms, unpublished data). Thus we validated our fluorometric approach by repeating each of the treatment parameters (i.e., amiloride, glibencamide, LPS, LPS+TEMPO, and NSC23766) using the Evans blue assay to measure changes in

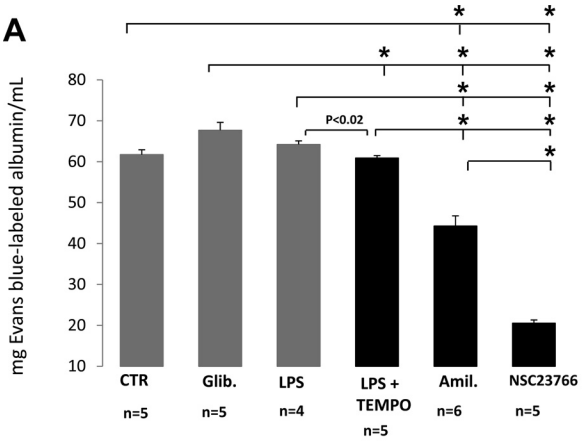

B

Alveolar Fluid Clearance-
% change in Evans blue-labeled albumin concentration instilled:

CTR	Glib.	LPS	LPS+ TEMPO	Amil.	NSC - 23766
22.05%	28.67%	24.28%	17.79%	-2.77%	-41.78%

Fig. 7. Changes in albumin protein concentration validate fluorometric data obtained from live animals. *A*: C57BL/6J mice challenged by IT instillation with either 100 μl glibenclamide (Glib.; 1 mM), LPS (1 mg/ml), LPS + TEMPO (250 μM), amiloride (Amil.; 1 mM), or NSC23766 (100 μM) combined with 5% BSA and Evans blue dye. Protein concentrations are reported after 60 min of treatment as mg/ml. Analysis of variance (Tukey's test) was used to determine significance between multiple groups; paired *t*-test was used determine statistical differences between LPS and LPS + TEMPO treatment; $*P < 0.05$ unless otherwise stated. Number of independent observations indicated on graph. *B*: alveolar fluid clearance expressed as % change in albumin instilled, calculated from AFC = $[(Vi-Vf)/Vi] \times 100$, as described in MATERIAL AND METHODS. The percent changes greater than average control values of 22.05% indicate enhanced rates of fluid clearance (glibenclamide), whereas negative percent changes are indicative of alveolar flooding (amiloride and NSC-23766). TEMPO attenuated LPS induced changes in AFC by ~6.5% in murine lungs.

albumin concentration as a measure of lung fluid clearance (44). These results are shown in Fig. 7 and verify that *1*) glibenclamide indeed increases AFC (compared with saline-instilled control) whether the results are measured by X-ray imaging or protein concentration measurements, *2*) amiloride and inhibition of Rac1 significantly decreases AFC (compared to saline-instilled control) whether the results are measured by X-ray imaging or protein concentration measurements, and *3*) sequestering ROS with TEMPO compound significantly attenuated the LPS-induced effect on lung fluid clearance. On the basis of these outcomes, we summarize that wet-to-dry weight determination and changes in albumin protein concentrations are useful metrics for measuring alveolar fluid clearance (at a single time point), and X-ray fluoroscopic imaging enables airway fluid to be quantified from live mice in real time (at multiple time points).

To better understand the time course of LPS-mediated effects on transport, we performed single-channel patch-clamp analysis on AT1 cells, which makes up > 95% of the surface area of the alveolar epithelium. The single-channel analysis in Fig. 6, *B–D*, shows that a 20 pS nonselective channel is activated following 1 μg/ml LPS treatment. We measured *N*Po, which is an electrophysiological measurement of sodium channel number (*N*) times open probability (Po). In LPS-treated patches, *N*Po activity increased from 0.14 ± 0.04 to 0.62 ± 0.23 ($n = 6$; $P < 0.05$). Importantly, 250 μM TEMPO treatment, subsequent to LPS, significantly decreased channel activity in the same cell-attached recordings with average *N*Po values decreasing to 0.04 ± 0.03. An increase in ENaC nonselective cation channel activity could explain the latent increase in lung fluid clearance induced by LPS between 210 and 240 min following IT instillation.

In vivo detection of lung ROS. Hydrocyanine 7 (Cy7) is a redox sensor that emits light in the near-infrared range (560–830 nm) upon interacting with ROS (26). To detect ROS production in vivo, we used a protocol that required two separate IT instillations. First, mice were IT instilled with either 1 mg/ml LPS, 1 mg/ml LPS + 100 μM NSC23766, 100 μM NSC23766 alone, or saline to stimulate or inhibit Nox2 activity. Four hours later, Cy7 was introduced by IT instillation and ROS-induced fluorescence was measured.

The Cy7 fluorescence signal, coregistered with white light illumination, was measured (Fig. 8*A*). Note the intensity scale bar that shows relative light intensities (RLU) correlated with ROS production. In Fig. 8*B*, average ROS levels were determined by calculating RLU values as photons per second per centimeter squared. We found that LPS enhanced ROS production compared with all other conditions tested, including IT instillation with saline alone, which also induced ROS, albeit lower than the level stimulated by LPS. Importantly, NSC23766 significantly decreased ROS production. Together, these findings indicate that LPS stimulates lung ROS release via a Rac1-dependent pathway.

DISCUSSION

A new fluoroscopic approach to assay relative lung fluid balance. Relative lung fluid volumes have been determined by measuring changes in albumin protein concentration (12, 36, 57) and also by comparing the lung wet-to-dry weight ratios (4, 12). Recently, Lewis et al. (30) reported the use of X-ray phase contrast in detecting lung aeration in rabbit pups delivered by caesarean section. In the present study, we expanded the use of X-ray imaging to assess lung fluid clearance in adult mice following saline challenge and were able to detect very small changes in lung fluid volume without euthanizing the animals. We are able to equate changes in lung fluid volume to ENaC activity because it has been shown that Na ions represent ~80% of the total ion transported in alveolar epithelial cells (24) and because amiloride (sodium channel blocker) significantly decreases the lungs' ability to resolve IT saline challenges. The fluorometric data shown in Fig. 3*A*, where amiloride instillation leads to alveolar flooding, is similar to the effects of instilling amiloride as reported by Matthay and colleagues (12) and Matalon and colleagues (47) using alternative approaches to measure lung fluid volume.

Our approach to measuring lung fluid balance involves tracheally instilling one lobe of the lung. Practically speaking, flooding one region (of otherwise healthy lung) in our procedure precludes the need to ventilate animals, which could introduce additional lung injury. Furthermore, animals that survive the saline challenge can be used for subsequent in vivo imaging studies (such as that shown in Fig. 7), or, as a follow-up, cell isolation. For our research purposes, this model of lung injury is useful for and represents a technical advancement for studying amiloride-inhibited transport

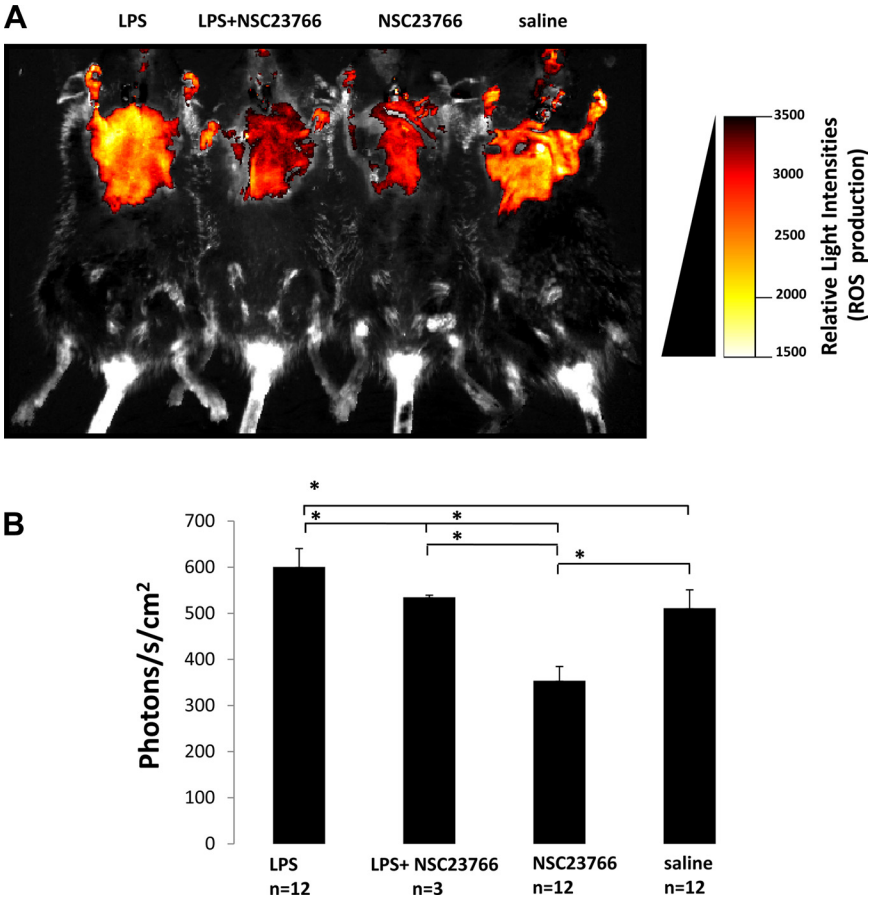

Fig. 8. In vivo detection of lung ROS. *A*: C57BL/6J mice challenged by IT instillation with either 100 μl 1 mg/ml LPS, 100 μl 1 mg/ml LPS + 100 μM NSC23766, 100 μM NSC23766, or 100 μl saline (control). Four hours after initial instillation, a second IT instillation of hydrocyanine dye was added to detect lung ROS production. *Left*: representative images of ROS produced by mice. *Right*: scale of relative light intensities (RLU) correlated with ROS production. *B*: average ROS was determined by calculating RLU values as photons $\cdot s^{-1} \cdot cm^{-2}$. LPS enhanced ROS production compared with all of the other conditions tested. NSC23766 significantly decreased ROS levels regardless of whether LPS was coinstilled. *$P < 0.05$. Number of observations reported under the graph, with LPS + NSC23766 observations lower than all other observations because of low viability in this treatment group.

in the lung. Several research groups, namely those of Matthay (27, 39), Matalon (13, 47), and O'Brodovich (51), have also similarly evaluated the rate of fluid clearance from isolated lobes of the lung. On the basis of these studies, and our wet-to-dry lung weight measurements, we presume that changes in fluid balance observed in one lobe of the lung represent changes in total lung fluid. Although beyond the scope of the present studies, the fluoroscopic approach to measuring lung fluid volume could be extended and applied to acute lung injury, asthma, and pneumonic animal models.

Rac1-mediated NADPH oxidase regulates lung fluid balance. We have recently reported that Nox2 is robustly expressed in the alveoli and plays an important role in regulating lung ENaC activity (49). Specifically, alveolar epithelial cells express Nox2 catalytic (gp^{91}phox and p^{22}phox) and cytoplasmic (p^{67}phox, p^{47}phox, and p^{40}phox) subunits, as well as Rac1, which controls subunit assembly. In this prior study, single-channel recordings treated with the Rac1 inhibitor NSC23766 significantly decreased production of O_2^- with a concomitant decrease in lung ENaC *N*Po. In the present study, we examined whether redox regulation of ENaC indeed translated into physiological changes in lung fluid volume. Interestingly, we found that Rac1 inhibition of Nox2 activity led to significant increases in lung fluid volume. In fact, compared with amiloride-instilled lungs, the NSC23766-treated lungs continued to take in water during the 240-min observation period. This suggests that Rac1, and perhaps other small-molecular-weight GTPases, may be regulating additional pathways or ion channels needed for reabsorption. As an alternative to pharmacologically inhibiting NADPH oxidase activity using NSC23766, we delivered saline challenges into the distal airways of Nox2-deficient mice. Similar to the observed effect in NSC23766-treated animals, disruption of normal NADPH oxidase activity significantly impaired fluid clearance, albeit at a later time point after IT challenge (between 95 and 240 min) and to a lesser extent than NSC23766. One possible explanation for the difference in response between NSC23766 and $Nox2^{-/-}$ animals is that other Nox isoforms may be compensating for the lack of normal Nox2 isoform in transgenic mice, whereas NSC23766 inhibition of Rac1 has the potential to alter all Rac-dependent Nox isoforms (Nox1–2) (20). In support of this, we have detected Nox1 and Nox4 expression in the alveolar epithelium using antibodies obtained from Dr. David Lambeth (Emory University) and Novus Biological (Littleton, CO), respectively (unpublished results). However, Nox isoform expression in the alveolar epithelium has not been systematically reported.

Using X-ray fluoroscopy, we observed a significant difference in the rate of fluid clearance in 12-wk-old animals (Fig. 3) and 8-wk-old animals (Fig. 5). We found that either younger animals were reabsorbing salt and water at a faster rate or the secretory pathways were less active in the 8-wk-old animals as opposed to 12-wk-old mice. Given the potential for age-related differences in lung fluid balance, we were careful to perform the appropriate age-matched controls for all of our experiments. Although beyond the scope of our present studies related to ROS regulation of lung ENaC and fluid balance, an additional advantage to using X-ray fluoroscopy to assess lung fluid clearance is that it offers the potential to track age-related changes in the capacity for lung fluid clearance in the same animals over time.

LPS regulates NSC and HSC channels and influences fluid clearance in the lungs. In addition to showing the physiological role of Rac-dependent NADPH oxidase activity, our studies provide mechanistic insight into the effect of LPS on sodium channel activity. As shown in Fig. 6 by in vivo imaging, LPS immediately impedes lung fluid reabsorption (up to ~75 min), yet lung fluid begins to steadily clear between 75 and 240 min following IT challenge. Moreover, TEMPO, a compound that sequesters ROS, antagonized this effect. These observations, coupled with single-channel analysis of the effect of LPS on ENaC expressed by AT1 cells, allowed us to correlate the effects of LPS on ion transport function with the acute effects of LPS on lung fluid clearance in vivo.

Prior to our studies, Boncoeur et al. (6) and Baines et al. (2) have shown that LPS inhibits highly selective amiloride-sensitive current in primary rat AT2 cells and human adenocarcinoma epithelial cells (H441) with characteristic type 2 phenotype. LPS inhibition of highly selective sodium channels (HSC) could indeed explain why, in our studies, tracheal instillation of LPS immediately decreased the rate of lung fluid clearance in C57BL/6J lung. Because HSC channels have Na^+/K^+ selectivity >40, inactivation of this family of channels may well lead to attenuation of lung fluid clearance at early times following IT instillation.

However, we also found that LPS stimulated nonselective cation channels in AT1 cells. Using single-channel recordings, Baines et al. (2) similarly reported that LPS increases the activity of NSC ENaC channels expressed by H441 airway cells (2). Likewise, Dodrill and Fedan (8) utilized Ussing chamber measurements to show that LPS increases Na^+ transport activity in airway epithelium. Activation of nonselective cation channels, with larger conductances of 19–24 pS, could explain the latent clearance of lung fluid in LPS-instilled animals between 75 and 240 min (Fig. 6). Because TEMPO inhibited this response, we conclude that LPS-mediated activation of nonselective sodium channels is ROS dependent. By combining in vivo imaging with single-channel measurements of ENaC, we are able to uniquely assess the effect of potentially therapeutic, or harmful, compounds and to gain understanding of the underlying molecular mechanisms.

Overall conclusion and clinical implications. We used three independent methods to disrupt superoxide release: TEMPO, Rac-1 inhibitor compound (NSC23766), and Nox2-deficient mice to show that decreases in O_2^- release lead to significant disruption of normal lung fluid balance. We measured these changes in vivo using a fluorometric assay, which provides a noninvasive alternative to measuring lung fluid volume in small rodents with high sensitivity. Moreover, our in vivo findings validated single-channel recordings showing that TEMPO and NSC23766 attenuated lung ENaC activity by demonstrating that this can disrupt the osmotic driving force needed for water reabsorption. Given the important role for NADPH oxidases in regulating alveolar fluid homeostasis, our data suggest that Nox (and Nox subunits) are likely to be key therapeutic targets with the capacity to reverse edematous lung injury or to promote fluid balance in hyperreabsorptive disorders, such as cystic fibrosis.

ACKNOWLEDGMENTS

The authors acknowledge the laboratory assistance of Elizabeth Brewer and David Trac.

GRANTS

This research was supported from National Institutes of Health Grants K99R00 HL09222601 awarded to M. N. Helms and P50-AA-013757 and R01-HL-083120 awarded to M. Koval.

DISCLOSURES

No conflicts of interest, financial or otherwise, are declared by the author(s).

CONTRIBUTIONS

P.G., L.J., M.K., and M.H. conception and design. P.G., M.K., A.K, and M.H. manuscript preparation. K.K and N.M. in vivo detection of ROS. P.G. and M.H. experiments and analysis.

REFERENCES

1. **Bai C, Biwersi J, Verkman AS, Matthay MA.** A mouse model to test the in vivo efficacy of chemical chaperones. *J Pharmacol Toxicol Methods* 40: 39–45, 1998.
2. **Baines DL, Albert AP, Hazell MJ, Gambling L, Woollhead AM, Dockrell ME.** Lipopolysaccharide modifies amiloride-sensitive Na^+ transport processes across human airway cells: role of mitogen-activated protein kinases ERK 1/2 and 5. *Pflügers Arch* 459: 451–463, 2010.
3. **Baines DL, Ramminger SJ, Collett A, Haddad JJ, Best OG, Land SC, Olver RE, Wilson SM.** Oxygen-evoked Na^+ transport in rat fetal distal lung epithelial cells. *J Physiol* 532: 105–113, 2001.
4. **Berthiaume Y, Staub NC, Matthay MA.** Beta-adrenergic agonists increase lung liquid clearance in anesthetized sheep. *J Clin Invest* 79: 335–343, 1987.
5. **Berthiaume Y, Voisin G, Dagenais A.** The alveolar type I cells: the new knight of the alveolus? *J Physiol* 572: 609–610, 2006.
6. **Boncoeur E, Tardif V, Tessier MC, Morneau F, Lavoie J, Gendreau-Berthiaume E, Grygorczyk R, Dagenais A, Berthiaume Y.** Modulation of epithelial sodium channel activity by lipopolysaccharide in alveolar type II cells: involvement of purinergic signaling. *Am J Physiol Lung Cell Mol Physiol* 298: L417–L426, 2010.
7. **Bove PF, Grubb BR, Okada SF, Ribeiro CM, Rogers TD, Randell SH, O'Neal WK, Boucher RC.** Human alveolar type II cells secrete and absorb liquid in response to local nucleotide signaling. *J Biol Chem* 285: 34939–34949, 2010.
8. **Dodrill MW, Fedan JS.** Lipopolysaccharide hyperpolarizes guinea pig airway epithelium by increasing the activities of the epithelial Na^+ channel and the Na^+-K^+ pump. *Am J Physiol Lung Cell Mol Physiol* 299: L550–L558, 2010.
9. **Driscoll KE, Costa DL, Hatch G, Henderson R, Oberdorster G, Salem H, Schlesinger RB.** Intratracheal instillation as an exposure technique for the evaluation of respiratory tract toxicity: uses and limitations. *Toxicol Sci* 55: 24–35, 2000.
10. **Eaton DC, Hamilton KL.** The amiloride-blockable sodium channel of epithelial tissue. *Ion Channels* 1: 251–282, 1988.
11. **Effros RM, Mason GR, Hukkanen J, Silverman P.** New evidence for active sodium transport from fluid-filled rat lungs. *J Appl Physiol* 66: 906–919, 1989.
12. **Fukuda N, Folkesson HG, Matthay MA.** Relationship of interstitial fluid volume to alveolar fluid clearance in mice: ventilated vs. in situ studies. *J Appl Physiol* 89: 672–679, 2000.
13. **Hall NG, Liu Y, Hickman-Davis JM, Davis GC, Myles C, Andrews EJ, Matalon S, Lang JD Jr.** Bactericidal function of alveolar macrophages in mechanically ventilated rabbits. *Am J Respir Cell Mol Biol* 34: 719–726, 2006.
14. **Hardiman KM, McNicholas-Bevensee CM, Fortenberry J, Myles CT, Malik B, Eaton DC, Matalon S.** Regulation of amiloride-sensitive Na^+ transport by basal nitric oxide. *Am J Respir Cell Mol Biol* 30: 720–728, 2004.
15. **Helms MN, Jain L, Self JL, Eaton DC.** Redox regulation of epithelial sodium channels examined in alveolar type 1 and 2 cells patch-clamped in lung slice tissue. *J Biol Chem* 283: 22875–22883, 2008.
16. **Helms MN, Liu L, Liang YY, Al-Khalili O, Vandewalle A, Saxena S, Eaton DC, Ma HP.** Phosphatidylinositol 3,4,5-trisphosphate mediates aldosterone stimulation of epithelial sodium channel (ENaC) and interacts with gamma-ENaC. *J Biol Chem* 280: 40885–40891, 2005.
17. **Helms MN, Self J, Bao HF, Job LC, Jain L, Eaton DC.** Dopamine activates amiloride-sensitive sodium channels in alveolar type I cells in

lung slice preparations. *Am J Physiol Lung Cell Mol Physiol* 291: L610–L618, 2006.
18. **Helms MN, Torres-Gonzalez E, Goodson P, Rojas M.** Direct tracheal instillation of solutes into mouse lung. *J Vis Exp* pii: 1941, 2010. doi:10.3791/1941.
19. **Hickman-Davis JM, McNicholas-Bevensee C, Davis IC, Ma HP, Davis GC, Bosworth CA, Matalon S.** Reactive species mediate inhibition of alveolar type II sodium transport during mycoplasma infection. *Am J Respir Crit Care Med* 173: 334–344, 2006.
20. **Hordijk PL.** Regulation of NADPH oxidases: the role of Rac proteins. *Circ Res* 98: 453–462, 2006.
21. **Hummler E, Barker P, Talbot C, Wang Q, Verdumo C, Grubb B, Gatzy J, Burnier M, Horisberger JD, Beermann F, Boucher R, Rossier BC.** A mouse model for the renal salt-wasting syndrome pseudohypoaldosteronism. *Proc Natl Acad Sci USA* 94: 11710–11715, 1997.
22. **Hummler E, Barker P, Gatzy J, Beermann F, Verdumo C, Schmidt A, Boucher R, Rossier BC.** Early death due to defective neonatal lung liquid clearance in αENaC-deficient mice. *Nat Genet* 12: 325–328, 1996.
23. **Kawahara T, Kohjima M, Kuwano Y, Mino H, Teshima-Kondo S, Takeya R, Tsunawaki S, Wada A, Sumimoto H, Rokutan K.** Helicobacter pylori lipopolysaccharide activates Rac1 and transcription of NADPH oxidase Nox1 and its organizer NOXO1 in guinea pig gastric mucosal cells. *Am J Physiol Cell Physiol* 288: C450–C457, 2005.
24. **Kim KJ, Suh DJ, Lubman RL, Danto SI, Borok Z, Crandall ED.** Studies on the mechanisms of active ion fluxes across alveolar epithelial cell monolayers. *J Tiss Cult Meth* 14: 187–194, 1992.
25. **Kim SY, Lee JG, Cho WS, Cho KH, Sakong J, Kim JR, Chin BR, Baek SH.** Role of NADPH oxidase-2 in lipopolysaccharide-induced matrix metalloproteinase expression and cell migration. *Immunol Cell Biol* 88: 197–204, 2010.
26. **Kundu K, Knight SF, Willett N, Lee S, Taylor WR, Murthy N.** Hydrocyanines: a class of fluorescent sensors that can image reactive oxygen species in cell culture, tissue, and in vivo. *Angew Chem Int Ed Engl* 48: 299–303, 2009.
27. **Laffon M, Jayr C, Barbry P, Wang Y, Folkesson HG, Pittet JF, Clerici C, Matthay MA.** Lidocaine induces a reversible decrease in alveolar epithelial fluid clearance in rats. *Anesthesiology* 96: 392–399, 2002.
28. **Lambeth DJ.** NOX enzymes and the biology of reactive oxygen. *Nat Rev* 4: 181–189, 2004.
29. **Lazrak A, Iles KE, Liu G, Noah DL, Noah JW, Matalon S.** Influenza virus M2 protein inhibits epithelial sodium channels by increasing reactive oxygen species. *FASEB J* 23: 3829–3842, 2009.
30. **Lewis RA, Yagi N, Kitchen MJ, Morgan MJ, Paganin D, Siu KK, Pavlov K, Williams I, Uesugi K, Wallace MJ, Hall CJ, Whitley J, Hooper SB.** Dynamic imaging of the lungs using x-ray phase contrast. *Phys Med Biol* 50: 5031–5040, 2005.
31. **Li T, Folkesson HG.** RNA interference for α-ENaC inhibits rat lung fluid absorption in vivo. *Am J Physiol Lung Cell Mol Physiol* 290: L649–L660, 2006.
32. **Ma HP, Chou CF, Wei SP, Eaton DC.** Regulation of the epithelial sodium channel by phosphatidylinositides: experiments, implications, and speculations. *Pflügers Arch* 455: 169–180, 2007.
33. **Mall M, Grubb BR, Harkema JR, O'Neal WK, Boucher RC.** Increased airway epithelial Na^+ absorption produces cystic fibrosis-like lung disease in mice. *Nat Med* 10: 487–493, 2004.
34. **Matalon S, Hardiman KM, Jain L, Eaton DC, Kotlikoff M, Eu JP, Sun J, Meissner G, Stamler JS.** Regulation of ion channel structure and function by reactive oxygen-nitrogen species. *Am J Physiol Lung Cell Mol Physiol* 285: L1184–L1189, 2003.
35. **McNeilly TN, Tennant P, Lujan L, Perez M, Harkiss GD.** Differential infection efficiencies of peripheral lung and tracheal tissues in sheep infected with Visna/maedi virus via the respiratory tract. *J Gen Virol* 88: 670–679, 2007.
36. **Norlin A, Lu LN, Guggino SE, Matthay MA, Folkesson HG.** Contribution of amiloride-insensitive pathways to alveolar fluid clearance in adult rats. *J Appl Physiol* 90: 1489–1496, 2001.
37. **Otulakowski G, Duan W, Gandhi S, O'Brodovich H.** Steroid and oxygen effects on eIF4F complex, mTOR, and ENaC translation in fetal lung epithelia. *Am J Respir Cell Mol Biol* 37: 457–466, 2007.
38. **Otulakowski G, Rafii B, Harris M, O'Brodovich H.** Oxygen and glucocorticoids modulate alphaENaC mRNA translation in fetal distal lung epithelium. *Am J Respir Cell Mol Biol* 34: 204–212, 2006.
39. **Pittet JF, Lu LN, Geiser T, Lee H, Matthay MA, Welch WJ.** Stress preconditioning attenuates oxidative injury to the alveolar epithelium of the lung following haemorrhage in rats. *J Physiol* 538: 583–597, 2002.
40. **Rafii B, Coutinho C, Otulakowski G, O'Brodovich H.** Oxygen induction of epithelial Na^+ transport requires heme proteins. *Am J Physiol Lung Cell Mol Physiol* 278: L399–L406, 2000.
41. **Rafii B, Tanswell AK, Otulakowski G, Pitkanen O, Belcastro-Taylor R, O'Brodovich H.** O_2-induced ENaC expression is associated with NF-κB activation and blocked by superoxide scavenger. *Am J Physiol Lung Cell Mol Physiol* 275: L764–L770, 1998.
42. **Ramminger SJ, Baines DL, Olver RE, Wilson SM.** The effects of P_{O_2} upon transepithelial ion transport in fetal rat distal lung epithelial cells. *J Physiol* 524: 539–547, 2000.
43. **Richard K, Ramminger SJ, Inglis SK, Olver RE, Land SC, Wilson SM.** O_2 can raise fetal pneumocyte Na^+ conductance without affecting ENaC mRNA abundance. *Biochem Biophys Res Commun* 305: 671–676, 2003.
44. **Sakuma T, Sagawa M, Hida M, Nambu Y, Osanai K, Toga H, Takahashi K, Ohya N, Matthay MA.** Time-dependent effect of pneumonectomy on alveolar epithelial fluid clearance in rat lungs. *J Thorac Cardiovasc Surg* 124: 668–674, 2002.
45. **Sheppard DN, Robinson KA.** Mechanism of glibenclamide inhibition of cystic fibrosis transmembrane conductance regulator Cl- channels expressed in a murine cell line. *J Physiol* 503: 333–346, 1997.
46. **Sheridan MB, Fong P, Groman JD, Conrad C, Flume P, Diaz R, Harris C, Knowles M, Cutting GR.** Mutations in the beta-subunit of the epithelial Na^+ channel in patients with a cystic fibrosis-like syndrome. *Hum Mol Genet* 14: 3493–3498, 2005.
47. **Song W, Wei S, Zhou Y, Lazrak A, Liu G, Londino JD, Squadrito GL, Matalon S.** Inhibition of lung fluid clearance and epithelial Na^+ channels by chlorine, hypochlorous acid, and chloramines. *J Biol Chem* 285: 9716–9728, 2010.
48. **Starcher B, Williams I.** A method for intratracheal instillation of endotoxin into the lungs of mice. *Lab Anim* 23: 234–240, 1989.
49. **Takemura Y, Goodson P, Bao HF, Jain L, Helms MN.** Rac1-mediated NADPH oxidase release of O_2^- regulates epithelial sodium channel activity in the alveolar epithelium. *Am J Physiol Lung Cell Mol Physiol* 298: L509–L520, 2010.
50. **Thome UH, Davis IC, Nguyen SV, Shelton BJ, Matalon S.** Modulation of sodium transport in fetal alveolar epithelial cells by oxygen and corticosterone. *Am J Physiol Lung Cell Mol Physiol* 284: L376–L385, 2003.
51. **Vidarsson L, Helm E, O'Brodovich H, Macgowan CK.** Visualizing water clearance in the lung with MRI. *Magn Reson Med* 60: 230–235, 2008.
52. **Wang HC, Zentner MD, Deng HT, Kim KJ, Wu R, Yang PC, Ann DK.** Oxidative stress disrupts glucocorticoid hormone-dependent transcription of the amiloride-sensitive epithelial sodium channel alpha-subunit in lung epithelial cells through ERK-dependent and thioredoxin-sensitive pathways. *J Biol Chem* 275: 8600–8609, 2000.
53. **Ware LB, Fang X, Wang Y, Sakuma T, Hall TS, Matthay MA.** Selected contribution: mechanisms that may stimulate the resolution of alveolar edema in the transplanted human lung. *J Appl Physiol* 93: 1869–1874, 2002.
54. **Wright JR, Dobbs LG.** Regulation of pulmonary surfactant secretion and clearance. *Annu Rev Physiol* 53: 395–414, 1991.
55. **Yeh TF, Lin HC, Chang CH, Wu TS, Su BH, Li TC, Pyati S, Tsai CH.** Early intratracheal instillation of budesonide using surfactant as a vehicle to prevent chronic lung disease in preterm infants: a pilot study. *Pediatrics* 121: e1310–e1318, 2008.
56. **Yu L, Bao HF, Self JL, Eaton DC, Helms MN.** Aldosterone-induced increases in superoxide production counters nitric oxide inhibition of epithelial Na channel activity in A6 distal nephron cells. *Am J Physiol Renal Physiol* 293: F1666–F1677, 2007.
57. **Yue G, Matalon S.** Mechanisms and sequelae of increased alveolar fluid clearance in hyperoxic rats. *Am J Physiol Lung Cell Mol Physiol* 272: L407–L412, 1997.
58. **Zhou Z, Duerr J, Johannesson B, Schubert SC, Treis D, Harm M, Graeber SY, Dalpke A, Schultz C, Mall MA.** The ENaC-overexpressing mouse as a model of cystic fibrosis lung disease. *J Cyst Fibros* 10, *Suppl* 2: S172–S182, 2011.